SoftwareX 12 (2020) 100567

Contents lists available at ScienceDirect

SoftwareX

journal homepage: www.elsevier.com/locate/softx

Original software publication

SpinUpFlowDescriptor: A MATLAB toolbox for ferrofluids materials under moderate and high amplitude and frequency of magnetic rotating fields in a spin-up geometry

Cristian Jimenez [a,*], Iván Amaya [b], Rodrigo Correa [a]

[a] Universidad Industrial de Santander, Escuela de Ingenierías Eléctrica, Electrónica y de Telecomunicaciones, Cra. 27 Calle 9, Bucaramanga, 680002, Colombia
[b] Tecnologico de Monterrey, School of Engineering and Sciences, Av. Eugenio Garza Sada, 2501 Sur, Mexico

ARTICLE INFO

Article history:
Received 17 June 2020
Received in revised form 2 July 2020
Accepted 3 July 2020

Keywords:
Spin diffusion theory
Ferrofluid
Rotating magnetic fields
Spin-up geometry

ABSTRACT

There is currently no unified theory for describing ferrofluid flow under a rotating magnetic field. Spin diffusion theory has been broadly studied. But it has been limited to scenarios of magnetic fields with low intensity, due to the approximations required for the analytical solution. SpinUpFlowDescriptor is a MATLAB software that solves the ferrohydrodynamic problem, using finite difference equations. Our software does not require simplifications that limit its validity. So, it can be used for different field intensities, as shown in the experiments. Moreover, our data depict a saturation phenomenon for the velocity profiles, previously unreported for the spin-up geometry.

Code metadata

Current code version	V1
Permanent link to code/repository used of this code version	https://github.com/ElsevierSoftwareX/SOFTX_2020_260
Code Ocean compute capsule	None
Legal Code License	**GNU Lesser General Public License v3.0**
Code versioning system used	Git
Software code languages, tools, and services used	MATLAB
Compilation requirements, operating environments & dependencies	MATLAB R2018a
If available Link to developer documentation/manual	https://github.com/cristian12144/Spin-Up-Geomtry.git
Support email for questions	cristian.camilo.jimenez@gmail.com

1. Motivation and significance

The theory of internal angular momentum diffusion (TIAMD) has been broadly studied in recent years. Focus has been given to validating its ability for predicting flow profiles for ferrofluids within diverse geometries [1–4]. Nonetheless, analytical solutions of the ferrohydrodynamic model reported in literature [1] fall short when compared against experimental data [5]. Even though such analytical solutions have been a good starting point for validating TIAMD, the required assumptions oversimplify the problem. For example, they limit the validity of the profiles achieved for Rotational Magnetic Fields (RMF) to those with low amplitude and frequency. This phenomenon is shown in [5], where the authors considered a cylindrical geometry containing the ferrofluid. The authors detected a significant difference between experimental profiles and those given by the analytical solution, especially at moderate and high values of field amplitude and frequency. Such a disagreement leads to the need of a different methodology for solving the TIAMD; one that does not require the currently used simplifications. Because of the aforementioned, in this work we present the SpinUpFlowDescriptor software, which has been developed in MATLAB. One application of such software is shown in [6]. There, our software was used for

* Corresponding author.
E-mail addresses: cristian.camilo.jimenez@gmail.com, cristian.jimenez@correo.uis.edu.co (C. Jimenez), iamaya2@tec.mx (I. Amaya), crcorrea@saber.uis.edu.co (R. Correa).

https://doi.org/10.1016/j.softx.2020.100567

numerically solving the TIAMD and to generate velocity profiles, $v_\theta(r)$ and $\omega_z(r)$, for a sample of ferrofluid being contained within a cylindrical device with infinite axial longitude (Fig. 1). Moreover, the process was subject to the action of RMF with moderate and high values of both, frequency and amplitude. In this way, we provide a tool for generating data that more closely resembles the experimental one.

2. Problem and background

Our proposed software tackles the problem of properly simulating the behaviour of ferrofluids under the effect of rotational magnetic fields (RMF) with moderate and high amplitude and frequency, and for a spin-up geometry. So, we now provide the background of the problem, as well as its mathematical formulation.

The ferrohydrodynamic model is comprised by two sets of equations: (a) hydrodynamic equations, which describe convective and diffusive transport phenomena of quantity of momentum; and (b) magnetic equations, which describe magnetization phenomena of nanoparticles, as well as the torque that tends to align particle magnetization with the external RMF [7].

2.1. Hydrodynamic equations

The set of hydrodynamic equations is given by the continuity equation for an incompressible ferrofluid, as well as by Cauchy linear movement equation and the balance equation of internal angular moment [8]:

$$\nabla \cdot \mathbf{v} = 0, \tag{1}$$

$$\rho \frac{D\mathbf{v}}{Dt} = -\nabla p + \rho \mathbf{g} + \mu_0 \mathbf{M} \cdot \nabla \mathbf{H} + 2\zeta (\nabla \times \boldsymbol{\omega}) + \eta_e \nabla^2 \mathbf{v}, \tag{2}$$

$$\rho \frac{D\boldsymbol{\omega}}{Dt} = \mu_0 \mathbf{M} \times \mathbf{H} + 2\zeta (\nabla \times \mathbf{v} - 2\boldsymbol{\omega}) + \left(\lambda' + \eta'\right) \nabla (\nabla \cdot \boldsymbol{\omega}) + \eta' \nabla^2 \boldsymbol{\omega}, \tag{3}$$

where $\mathbf{v}$ is the mass average linear velocity, $\boldsymbol{\omega}$ is the rotation velocity of magnetic particles, and p represents the pressure of the system. Similarly, ρ is the density of the ferrofluid, $\mathbf{g}$ is the gravitational acceleration, and $\mathbf{I}$ is the density of the inertia moment of the suspension. Moreover, $\mathbf{M}$ stands for the magnetization vector, $\mathbf{H}$ is the intensity of the applied magnetic field, η is the shear viscosity, η' is the shear coefficient of spin viscosity (sc-sv), λ is the volumetric viscosity, and λ' is the bulk coefficient of spin viscosity (bc-sv). Finally, ζ is the vortex viscosity, which was defined by Brenner [9] as in Eq. (4).

$$\zeta = 1.5 \phi_h \eta_0. \tag{4}$$

The previous equation is valid at the limit of infinite dilution. In the equation, ϕ_h stands for the hydrodynamic volumetric fraction of magnetic particles within the suspension, and η_0 is the dynamic viscosity of the fluid that carries magnetic particles.

For the magnetic body-force density, $\mathbf{F}$, Cowley and Rosensweig [10] proposed Eq. (5), where v is a measure of per unit mass so that vM represents the magnetic moment per unit mass and nv would stand for the number of particles per unit mass. Now, for a diluted sample, average particle magnetization only depends on the RMF, unless magnetostriction effects are relevant [7]. Nonetheless, under the effect of an RMF with low intensity and frequency, it is common to neglect magnetostriction effects [1,5]. Therefore, in our case vM does not depend on v, and thus the integral term of Eq. (5) vanishes [7]. Consequently, the magnetic body-force density becomes as in Eq. (6). Bear in mind that such a definition is the one implemented to arrive at Eq. (2) [8].

$$\mathbf{F} = \mu_0 (\mathbf{M}, \nabla) \mathbf{H} - \nabla \left\{ \mu_0 \int_0^H \left. \frac{\partial (vM)}{\partial v} \right|_{H,T} dH \right\}. \tag{5}$$

$$\mathbf{F} = \mu_0 (\mathbf{M}, \nabla) \mathbf{H}. \tag{6}$$

Note that Eq. (6) is an expression that may affect the accuracy of results. This is particularly true when the ferrofluid is not diluted or when magnetostriction cannot be disregarded. The latter occurs when the RMF has a high amplitude and frequency.

Parting from Eqs. (1)–(3) we now present the dimensionless hydrodynamic equations, Eqs. (7)–(9), which have been implemented along with the regular perturbation method [1] for the analytic solution of the model. This solution is only valid for low amplitude and frequency values of the RMF. These values differ from experimental conditions found in literature [1,5]. This situation has represented a drawback for evaluating the TIAMD as a tool for describing flow profiles.

$$\widetilde{\nabla} \cdot \tilde{\mathbf{v}} = 0, \tag{7}$$

$$Re_v \frac{D\tilde{\mathbf{v}}}{Dt} = \frac{\zeta}{\widetilde{\Omega} \eta} \widetilde{\mathbf{M}} \cdot \widetilde{\nabla} \widetilde{\mathbf{H}} - \widetilde{\nabla} \tilde{p} + \frac{2\zeta}{\eta} \widetilde{\nabla} \times \tilde{\boldsymbol{\omega}} + \frac{\eta_e}{\eta} \widetilde{\nabla}^2 \tilde{\mathbf{v}}, \tag{8}$$

$$Re_\omega \frac{D\tilde{\boldsymbol{\omega}}}{Dt} = \frac{1}{\widetilde{\Omega}} \left(\widetilde{\mathbf{M}} \times \widetilde{\mathbf{H}}\right) + 2\widetilde{\nabla} \times \tilde{\mathbf{v}} - 4\tilde{\boldsymbol{\omega}} + \frac{4\eta}{\eta_e} \left(\frac{1}{ve^2} + \frac{1}{\kappa^2}\right) \times \widetilde{\nabla} \left(\widetilde{\nabla} \cdot \tilde{\boldsymbol{\omega}}\right) + \frac{4\eta}{\eta_e \kappa^2} \widetilde{\nabla}^2 \tilde{\boldsymbol{\omega}}. \tag{9}$$

In Eq. (9), $\kappa^2 = {}^{4\eta\zeta R_0^2}/_{\eta' \eta_e}$ is a variable with no physical meaning, and is related to sc-sv (η'). Similarly, $ve^2 = {}^{4\eta\zeta R_0^2}/_{\lambda' \eta_e}$ is related to bc-sv (λ'). Moreover, in Eqs. (8) and (9), $Re_v = \frac{\rho R_0^2}{\eta} \left(\frac{\mu_0 \chi K^2 \widetilde{\Omega}}{\zeta}\right)$ and $Re_\omega = \frac{\rho I}{\zeta} \left(\frac{\mu_0 \chi K^2 \widetilde{\Omega}}{\zeta}\right)$ represent translational and rotational Reynolds numbers, respectively.

When considering an analysis for low Reynolds numbers ($Re \ll 1$), the convective terms in Eqs. (8) and (9), $\tilde{\mathbf{v}} \cdot \widetilde{\nabla} \tilde{\mathbf{v}}$ and $\tilde{\mathbf{v}} \cdot \widetilde{\nabla} \tilde{\boldsymbol{\omega}}$, nullify. Hence, such equations can be restated as shown in Eqs. (10) and (11).

$$\frac{\zeta}{\widetilde{\Omega} \eta} \widetilde{\mathbf{M}} \cdot \widetilde{\nabla} \widetilde{\mathbf{H}} - \widetilde{\nabla} \tilde{p} + \frac{2\zeta}{\eta} \widetilde{\nabla} \times \tilde{\boldsymbol{\omega}} + \frac{\eta_e}{\eta} \widetilde{\nabla}^2 \tilde{\mathbf{v}} = \mathbf{0}, \tag{10}$$

$$\frac{1}{\widetilde{\Omega}} \left(\widetilde{\mathbf{M}} \times \widetilde{\mathbf{H}}\right) + 2\widetilde{\nabla} \times \tilde{\mathbf{v}} - 4\tilde{\boldsymbol{\omega}} + \frac{4\eta}{\eta_e} \left(\frac{1}{ve^2} + \frac{1}{\kappa^2}\right) \widetilde{\nabla} \left(\widetilde{\nabla} \cdot \tilde{\boldsymbol{\omega}}\right) + \frac{4\eta}{\eta_e \kappa^2} \widetilde{\nabla}^2 \tilde{\boldsymbol{\omega}} = \mathbf{0}. \tag{11}$$

2.2. Magnetic equations

The system of magnetic equations is made up by equations, Sh-72 and MRSh-74, which describe the magnetization relaxation of a magnetic particle exposed to an external RMF. Likewise, the magnetization balance equation is included in such a system. This equation describes the magnetization saturation phenomenon when subject to an external RMF. Such a phenomenon is disregarded in the approximate model that is solved analytically [1]. In the aforementioned work, the magnetization is described as a variable proportional to the applied external field. Hence, $\mathbf{M} = \chi \mathbf{H}$. This assumption is only valid at low intensities of the RMF, where magnetization behaves linearly w.r.t. the external field $\mathbf{H}$ [5]. The system of magnetic equations is completed by Gauss law for magnetic fields and the generalized Ampère law. They are both members of Maxwell equations. The whole set of magnetic equations is given in Eqs. (12)–(16), along with their dimensions.

$$\frac{\partial \mathbf{M}}{\partial t} + \nabla \cdot (\mathbf{vM}) = \boldsymbol{\omega} \times \mathbf{M} - \frac{\mathbf{1}}{\tau} (\mathbf{M} - \mathbf{M_0}), \tag{12}$$

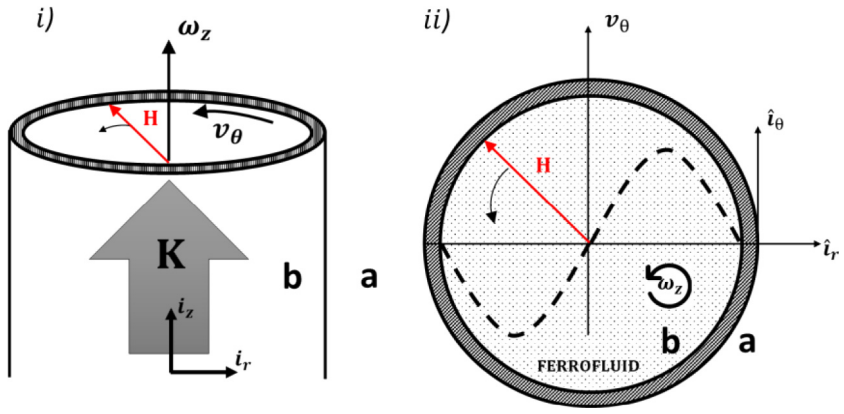

Fig. 1. Schematic diagram of a ferrofluid flowing within a cylinder with infinite axial longitude due to a uniform RMF **H**. The field rotates around the axial $\tilde{\boldsymbol{z}}$-axis, and is generated by the winding of a triple-phase induction motor with two poles. (*i*) front view. (*ii*) top view.

$$\frac{\partial \mathbf{M}}{\partial t} + \nabla \cdot (\mathbf{vM}) = \boldsymbol{\omega} \times \mathbf{M} - \frac{\mathbf{H}\left[\mathbf{H} \cdot (\mathbf{M} - \mathbf{M_0})\right]}{\tau_{\parallel} |\mathbf{H}|^2} - \frac{\mathbf{H} \times (\mathbf{M} \times \mathbf{H})}{\tau_{\perp} |\mathbf{H}|^2}, \tag{13}$$

$$\tau_{\parallel} = \frac{dlnL(\alpha)}{dln(\alpha)} \cdot \tau_B, \qquad \tau_{\perp} = \frac{2L(\alpha)}{\alpha - L(\alpha)} \cdot \tau_B, \tag{14}$$

$$\nabla \times \mathbf{H} = \mathbf{0}, \qquad \nabla \cdot (\mathbf{H} + \mathbf{M}) = 0\,, \tag{15}$$

$$\frac{\mathbf{M_0}}{\phi M_d} = L(\alpha)\frac{\mathbf{H}}{|\mathbf{H}|} = \left[\coth(\alpha) - \frac{1}{\alpha}\right]\frac{\mathbf{H}}{|\mathbf{H}|}, \quad \alpha = \frac{\mu_0 M_d |\mathbf{H}| V_c}{k_B T}. \tag{16}$$

It is important to remark that $\mathbf{M_0}$ stands for the saturation magnetization, whilst τ_B is the time of magnetization relaxation, where we assume that the relaxation mechanism yields a rotation of the magnetic particle. This means that we assume a Brownian mechanism of relaxation. So, $\tau = \tau_B$. Moreover, D/Dt is the material derivative, $\tau_{\parallel}$ is the parallel relaxation time, $\tau_{\perp}$ is the perpendicular relaxation time, as defined by Martsenyuk et al. [11]. Similarly, M_d is the magnetization across the domain, ϕ is the volumetric fraction of nanomagnetic particles, $L(\alpha)$ and α represent Langevin equation and coefficient, respectively, V_c is the volume of the magnetic particle, k_B is Boltzmann constant and T is the absolute temperature of the system.

Eqs. (17)–(20) show the dimensionless magnetic system, where $\varepsilon = \frac{\mu_0 \chi K^2 \tau}{\zeta} = \frac{2}{3}\alpha^2$ is known as the perturbation parameter, which is needed for the analytic solution of the model [1].

$$\widetilde{\Omega}\frac{D\widetilde{\mathbf{M}}}{D\tilde{t}} + \widetilde{\Omega}\varepsilon\tilde{\mathbf{v}} \cdot \widetilde{\nabla}\widetilde{\mathbf{M}} = \widetilde{\Omega}\varepsilon\tilde{\boldsymbol{\omega}} \times \widetilde{\mathbf{M}} - \widetilde{\mathbf{M}} + \frac{\mathbf{M_0}}{\chi K}, \tag{17}$$

$$\widetilde{\Omega}\frac{D\widetilde{\mathbf{M}}}{D\tilde{t}} = \widetilde{\Omega}\varepsilon\tilde{\boldsymbol{\omega}} \times \widetilde{\mathbf{M}} + \frac{\widetilde{\mathbf{H}}\left(\widetilde{\mathbf{H}} \cdot \widetilde{\mathbf{M}}\right)}{\left|\widetilde{\mathbf{H}}\right|^2}\left(\frac{1}{B_{\perp}} - \frac{1}{B_{\parallel}}\right) + \frac{3\widetilde{\mathbf{H}}\varphi\left(\widetilde{H}_r, \widetilde{H}_\theta\right)}{B_{\parallel}} - \frac{\widetilde{\mathbf{M}}}{B_{\perp}}, \tag{18}$$

$$\widetilde{\nabla} \times \widetilde{\mathbf{H}} = \mathbf{0}, \tag{19}$$

$$\widetilde{\nabla} \cdot \left(\chi\widetilde{\mathbf{M}} + \widetilde{\mathbf{H}}\right) = 0. \tag{20}$$

In a similar way, the dimensionless constants of both, parallel and perpendicular, relaxation times, $B_{\parallel}$ and $B_{\perp}$, respectively, are now given, along with function $\varphi = L(\alpha)/\alpha$, which has no physical meaning, in Eqs. (21)–(23).

$$B_{\parallel} = \frac{\tau_{\parallel}}{\tau_B} = \frac{d\ln L(\alpha)}{d\ln(\alpha)}, \tag{21}$$

$$B_{\perp} = \frac{\tau_{\perp}}{\tau_B} = \frac{2L(\alpha)}{\alpha - L(\alpha)}, \tag{22}$$

$$\varphi\left(\widetilde{H}_r, \widetilde{H}_\theta\right) = \frac{\coth(\alpha)}{\alpha} - \frac{1}{\alpha^2} = \frac{\coth\left(\sqrt{\frac{3}{2}\varepsilon\left(\widetilde{H}_r^2 + \widetilde{H}_\theta^2\right)}\right)}{\sqrt{\frac{3}{2}\varepsilon\left(\widetilde{H}_r^2 + \widetilde{H}_\theta^2\right)}} - \frac{2}{3\varepsilon\left(\widetilde{H}_r^2 + \widetilde{H}_\theta^2\right)}. \tag{23}$$

Finally, Langevin parameter (α) can be defined as shown in Eq. (24).

$$\alpha = \sqrt{\frac{3}{2}\varepsilon\left|\widetilde{\mathbf{H}}\right|^2} = \sqrt{\frac{3}{2}\varepsilon\left(\widetilde{H}_r^2 + \widetilde{H}_\theta^2\right)}. \tag{24}$$

3. Software framework

Fig. 2 shows a flow diagram that corresponds with the process followed by the SpinUpFlowDescriptor software. So, we move on to describe the major functionalities of the software.

The methodology can be summarized as follows. Initially, the features of the ferrofluid sample are identified, as well as the simulation parameters. Next, an initial value of the average magnetic torque, $\left\langle \tilde{l}_z \right\rangle_t^n$, is used to calculate the first velocity profiles, $\tilde{v}_\theta^n(\tilde{r})$ and $\widetilde{\omega}_z^n(\tilde{r})$. From these values, and using the magnetic equations, the components of magnetic field intensity and magnetization $(\widetilde{H}_r^n(\tilde{r},\tilde{\theta},\tilde{t}), \widetilde{M}_\theta^n(\tilde{r},\tilde{\theta},\tilde{t}), \widetilde{M}_r^n(\tilde{r},\tilde{\theta},\tilde{t}), \widetilde{M}_\theta^n(\tilde{r},\tilde{\theta},\tilde{t}))$, are estimated. Through them, a new average torque value, $\left\langle \tilde{l}_z \right\rangle_t^{n+1}$, is calculated for assessing convergence with $\left|\left\langle \tilde{l}_z \right\rangle_t^{n+1} - \left\langle \tilde{l}_z \right\rangle_t^{n}\right| \leq \varepsilon$. Should the torque value converge, an output with profiles $\tilde{v}_\theta^n(\tilde{r})$ and $\widetilde{\omega}_z^n(\tilde{r})$ is given to the user. Otherwise, velocity profiles are recalculated with the new torque value, yielding $\tilde{v}_\theta^{n+1}(\tilde{r})$ and $\widetilde{\omega}_z^{n+1}(\tilde{r})$. The magnetic problem is solved anew and convergence is recalculated.

We now define each block of our proposed approach, considering the functions incorporated to the software.

3.1. Initial values

This block includes reading the parameters of the ferrofluid sample. Also, the cylindrical container is discretized based on the number of spatial (radials, *nder*, and angulars, *ndeθ*) and temporal (*ndt*) nodes, as shown in Eqs. (25)–(27) and Fig. 3.

$$\Delta\tilde{r} = \frac{1}{nder - 1}, \tag{25}$$

$$\Delta\theta = \frac{2 \cdot \pi}{ndeθ}, \tag{26}$$

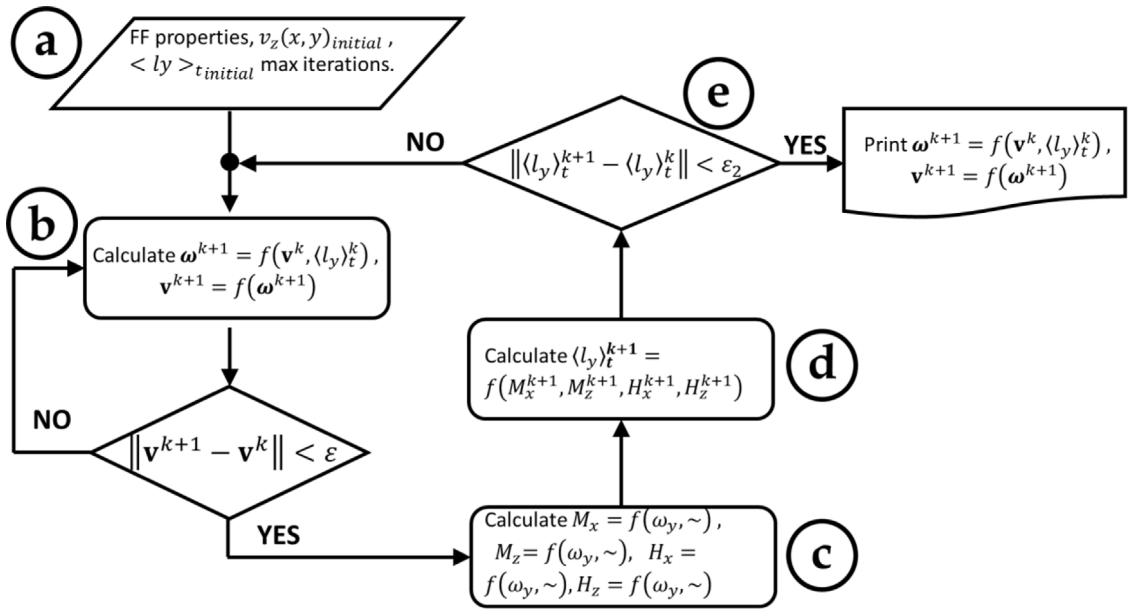

Fig. 2. Flow diagram of the SpinUpFlowDescriptor software for solving the ferrohydrodynamic problem of the TIAMD.

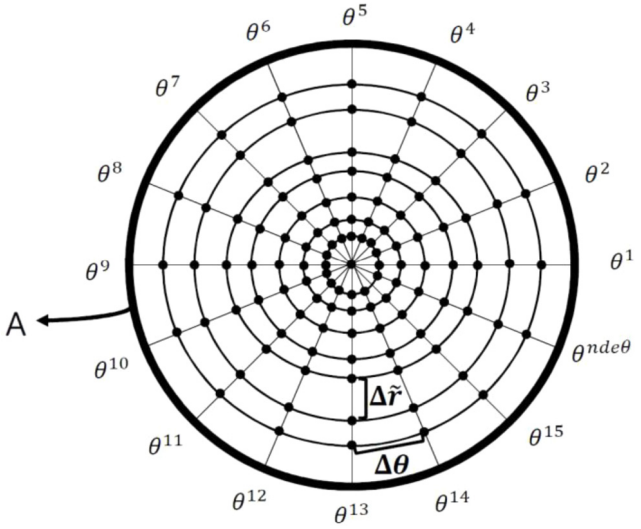

Fig. 3. Discretization scheme in the radial and azimuthal directions of a cylindrical container with infinite length in the axial longitude, $\tilde{\boldsymbol{z}}$. Black circles represent nodes where the physical system has been discretized. Moreover, ***nder*** and ***ndeθ*** stand for the number of spatial nodes in the $\tilde{\boldsymbol{r}}$ and $\boldsymbol{\theta}$ coordinates, respectively. These values are user-defined. The example shown considers ***nder*** $= \mathbf{9}$ and ***ndeθ*** $= \mathbf{16}$. A represents the cylinder wall at $\tilde{\boldsymbol{r}} = \mathbf{1}$.

$$\Delta\tilde{t} = \frac{\tilde{t}}{ndt - 1}. \tag{27}$$

3.2. Hydrodynamic stage

This block calculates the solution to the hydrodynamic problem $[\tilde{v}_\theta(\tilde{r})$ and $\widetilde{\omega}_z(\tilde{r})]$. The system of equations comprises the azimuth component of linear momentum balance, Eq. (28), and the vertical component of internal angular momentum conservation, Eq. (29).

$$\frac{\eta_e}{\eta}\frac{d}{d\tilde{r}}\left[\frac{1}{\tilde{r}}\frac{d}{d\tilde{r}}\left(\tilde{r}\tilde{v}_\theta\right)\right] - 2\frac{\zeta}{\eta}\frac{d\widetilde{\omega}_z}{d\tilde{r}} = 0, \tag{28}$$

$$\frac{2}{\tilde{r}}\frac{d}{d\tilde{r}}\left(\tilde{r}\tilde{v}_\theta\right) - 4\widetilde{\omega}_z + \frac{4\eta}{\eta_e\kappa^2}\frac{1}{\tilde{r}}\frac{d}{d\tilde{r}}\left(\tilde{r}\frac{d\widetilde{\omega}_z}{d\tilde{r}}\right) = -\frac{\left\langle\tilde{l}_z\right\rangle_t}{\widetilde{\Omega}}. \tag{29}$$

The solution of the hydrodynamic differential equations is carried out through finite differences. For the discretized equations, i represents the radial nodes in which the cylinder from Fig. 3 has been discretized.

$$\frac{\eta_e}{\eta}\left(\frac{-\tilde{v}_{\theta,i}}{\tilde{r}_i^2} + \frac{\tilde{v}_{\theta,i-1} - 2\tilde{v}_{\theta,i} - \tilde{v}_{\theta,i+1}}{\Delta\tilde{r}^2}\right) - \frac{\zeta}{\eta}\left(\frac{\widetilde{\omega}_{z,i+1} - \widetilde{\omega}_{z,i-1}}{2\Delta\tilde{r}}\right) = 0, \tag{30}$$

$$2\frac{\tilde{v}_{\theta,i}}{\tilde{r}_i} + \frac{\tilde{v}_{\theta,i+1} - \tilde{v}_{\theta,i-1}}{2\Delta\tilde{r}} - 4\widetilde{\omega}_{z,i} + \frac{4\eta}{\eta_e\kappa^2}\left(\frac{1}{\tilde{r}_i}\frac{\widetilde{\omega}_{z,i+1} - \widetilde{\omega}_{z,i-1}}{2\Delta\tilde{r}} + \frac{\widetilde{\omega}_{z,i-1} - 2\widetilde{\omega}_{z,i} + \widetilde{\omega}_{z,i+1}}{\Delta\tilde{r}^2}\right) = -\frac{\left\langle\tilde{l}_z\right\rangle_{t,i}}{\widetilde{\Omega}}. \tag{31}$$

Based on the coefficients from Eqs. (30) and (31), the set of algebraic equations is operated in matrix form, as follows:

$$\mathbf{A}\cdot\mathbf{x} = \mathbf{b}. \tag{32}$$

In Eq. (32), **A** represents the matrix of coefficients for the discretized equations, while **x** stands for the translational and rotational velocities, $\tilde{\mathbf{v}}_{\theta,i}$ and $\widetilde{\boldsymbol{\omega}}_{z,i}$, respectively.

3.3. Magnetic stage

In this block the software gathers the intensity of the applied magnetic field, $\widetilde{\mathbf{H}}(\tilde{r},\theta,\tilde{t})$, and the particles magnetization, $\widetilde{\mathbf{M}}(\tilde{r},\theta,\tilde{t})$, for each instant of the simulation. To this end, it implements the radial and angular components of the magnetization equations, i.e. Eqs. (33) and (34), respectively. This is merged with Gauss law for the magnetic field, Eq. (35), and Ampère

generalized current law, Eq. (36).

$$\widetilde{\Omega}\frac{\partial \widetilde{M}_r}{\partial \tilde{t}} + \widetilde{\Omega}\varepsilon\tilde{v}_\theta\left(\frac{1}{\tilde{r}}\frac{\partial \widetilde{M}_r}{\partial\theta} - \frac{\widetilde{M}_\theta}{\tilde{r}}\right) = -\widetilde{\Omega}\varepsilon\widetilde{\omega}_z\widetilde{M}_\theta + \frac{\widetilde{H}_r\left(\widetilde{H}_r\widetilde{M}_r + \widetilde{H}_\theta\widetilde{M}_\theta\right)}{\widetilde{H}_r{}^2 + \widetilde{H}_\theta{}^2}\left(\frac{1}{B_\perp} - \frac{1}{B_\parallel}\right) + \frac{3\widetilde{H}_r\varphi\left(\widetilde{H}_r,\widetilde{H}_\theta\right)}{B_\parallel} - \frac{\widetilde{M}_r}{B_\perp}, \tag{33}$$

$$\widetilde{\Omega}\frac{\partial \widetilde{M}_\theta}{\partial \tilde{t}} + \widetilde{\Omega}\varepsilon\tilde{v}_\theta\left(\frac{1}{\tilde{r}}\frac{\partial \widetilde{M}_\theta}{\partial\theta} + \frac{\widetilde{M}_r}{\tilde{r}}\right) = +\widetilde{\Omega}\varepsilon\widetilde{\omega}_z\widetilde{M}_r + \frac{\widetilde{H}_\theta\left(\widetilde{H}_r\widetilde{M}_r + \widetilde{H}_\theta\widetilde{M}_\theta\right)}{\widetilde{H}_r{}^2 + \widetilde{H}_\theta{}^2}\left(\frac{1}{B_\perp} - \frac{1}{B_\parallel}\right) + \frac{3\widetilde{H}_\theta\varphi\left(\widetilde{H}_r,\widetilde{H}_\theta\right)}{B_\parallel} - \frac{\widetilde{M}_\theta}{B_\perp}, \tag{34}$$

$$\widetilde{H}_\theta + \tilde{r}\frac{\partial \widetilde{H}_\theta}{\partial \tilde{r}} - \frac{\partial \widetilde{H}_r}{\partial\theta} = 0, \tag{35}$$

$$\widetilde{H}_r + \tilde{r}\frac{\partial \widetilde{H}_r}{\partial \tilde{r}} + \frac{\partial \widetilde{H}_\theta}{\partial\theta} = -\chi\left(\widetilde{M}_r + \tilde{r}\frac{\partial \widetilde{M}_r}{\partial \tilde{r}} + \frac{\partial \widetilde{M}_\theta}{\partial\theta}\right). \tag{36}$$

Now, Eqs. (23), (33)–(36) can be discretized as follows in Eqs. (37)–(41).

$$\widetilde{\Omega}\frac{\widetilde{M}^{j,k}_{r,i} - \widetilde{M}^{j,k-1}_{r,i}}{\Delta\tilde{t}} + \frac{\widetilde{\Omega}\varepsilon\tilde{v}_{\theta,i}}{\tilde{r}_i}\left(\frac{\widetilde{M}^{j,k}_{r,i} - \widetilde{M}^{j-1,k}_{r,i}}{\Delta\theta} - \widetilde{M}^{j,k}_{\theta,i}\right) = -\widetilde{\Omega}\varepsilon\widetilde{\omega}_{z,i}\widetilde{M}^{j,k}_{\theta,i} + \frac{\widetilde{H}^{j,k}_{r,i}\left(\widetilde{H}^{j,k}_{r,i}\widetilde{M}^{j,k}_{r,i} + \widetilde{H}^{j,k}_{\theta,i}\widetilde{M}^{j,k}_{\theta,i}\right)}{\left(\widetilde{H}^{j,k}_{r,i}\right)^2 + \left(\widetilde{H}^{j,k}_{\theta,i}\right)^2}\left(\frac{1}{B_\perp} - \frac{1}{B_\parallel}\right) + \frac{3\widetilde{H}^{j,k}_{r,i}\varphi\left(\widetilde{H}^{j,k}_{r,i},\widetilde{H}^{j,k}_{\theta,i}\right)}{B_\parallel} - \frac{\widetilde{M}^{j,k}_{r,i}}{B_\perp}, \tag{37}$$

$$\widetilde{\Omega}\frac{\widetilde{M}^{j,k}_{\theta,i} - \widetilde{M}^{j,k-1}_{\theta,i}}{\Delta\tilde{t}} + \frac{\widetilde{\Omega}\varepsilon\tilde{v}_{\theta,i}}{\tilde{r}_i}\left(\frac{\widetilde{M}^{j,k}_{\theta,i} - \widetilde{M}^{j-1,k}_{\theta,i}}{\Delta\theta} + \widetilde{M}^{j,k}_{r,i}\right) = +\widetilde{\Omega}\varepsilon\widetilde{\omega}_{z,i}\widetilde{M}^{j,k}_{r,i} + \frac{\widetilde{H}^{j,k}_{\theta,i}\left(\widetilde{H}^{j,k}_{r,i}\widetilde{M}^{j,k}_{r,i} + \widetilde{H}^{j,k}_{\theta,i}\widetilde{M}^{j,k}_{\theta,i}\right)}{\left(\widetilde{H}^{j,k}_{r,i}\right)^2 + \left(\widetilde{H}^{j,k}_{\theta,i}\right)^2}\left(\frac{1}{B_\perp} - \frac{1}{B_\parallel}\right) + \frac{3\widetilde{H}^{j,k}_{\theta,i}\varphi\left(\widetilde{H}^{j,k}_{r,i},\widetilde{H}^{j,k}_{\theta,i}\right)}{B_\parallel} - \frac{\widetilde{M}^{j,k}_{\theta,i}}{B_\perp}, \tag{38}$$

$$\varphi\left(\widetilde{H}^{j,k}_{r,i},\widetilde{H}^{j,k}_{\theta,i}\right) = \frac{\coth\left(\sqrt{\frac{3}{2}\varepsilon\left[\left(\widetilde{H}^{j,k}_{r,i}\right)^2 + \left(\widetilde{H}^{j,k}_{\theta,i}\right)^2\right]}\right)}{\sqrt{\frac{3}{2}\varepsilon\left[\left(\widetilde{H}^{j,k}_{r,i}\right)^2 + \left(\widetilde{H}^{j,k}_{\theta,i}\right)^2\right]}} - \frac{2}{3\varepsilon\left[\left(\widetilde{H}^{j,k}_{r,i}\right)^2 + \left(\widetilde{H}^{j,k}_{\theta,i}\right)^2\right]}, \tag{39}$$

$$\widetilde{H}^{j,k}_{\theta,i} + \tilde{r}_i\frac{\widetilde{H}^{j,k}_{\theta,i} - \widetilde{H}^{j,k}_{\theta,i-1}}{\Delta\tilde{r}} - \frac{\widetilde{H}^{j,k}_{r,i} - \widetilde{H}^{j-1,k}_{r,i}}{\Delta\theta} = 0, \tag{40}$$

$$\widetilde{H}^{j,k}_{r,i} + \tilde{r}_i\frac{\widetilde{H}^{j,k}_{r,i} - \widetilde{H}^{j,k}_{r,i-1}}{\Delta\tilde{r}} + \frac{\widetilde{H}^{j,k}_{\theta,i} - \widetilde{H}^{j-1,k}_{\theta,i}}{\Delta\theta} = -\chi\left(\widetilde{M}^{j,k}_{r,i} + \tilde{r}_i\frac{\widetilde{M}^{j,k}_{r,i} - \widetilde{M}^{j,k}_{r,i-1}}{\Delta\tilde{r}} + \frac{\widetilde{M}^{j,k}_{\theta,i} - \widetilde{M}^{j-1,k}_{\theta,i}}{\Delta\theta}\right). \tag{41}$$

Next, Maxwell equations, Eqs. (40) and (41), are solved using $\widetilde{M}_r\left(\tilde{r},\theta,\tilde{t}\right)$ and $\widetilde{M}_\theta\left(\tilde{r},\theta,\tilde{t}\right)$. So, equations are sorted and solved as laid out in Eq. (32).

3.4. Torque calculation

Instant torque is calculated through Eq. (42). Moreover, and considering that hydrodynamic equations are solved for the steady state (i.e. disregarding transient phenomena), the average torque, $\left\langle\tilde{l}_z\right\rangle_t$, can also be calculated, as shown in Eq. (43).

$$\tilde{l}_z\left(\tilde{r},\theta,\tilde{t}\right) = \left(\widetilde{\mathbf{M}}\times\widetilde{\mathbf{H}}\right)_z = \widetilde{M}_r\widetilde{H}_\theta - \widetilde{M}_\theta\widetilde{H}_r. \tag{42}$$

$$\left\langle\tilde{l}_z\right\rangle_t = \frac{1}{\tilde{t}}\int_0^{\tilde{t}}\tilde{l}_z\left(\tilde{r},\theta,\tilde{t}\right)d\tilde{t}. \tag{43}$$

Then, Eqs. (42) and (43) are discretized, based on the data from block c, as shown in Eqs. (44) and (45).

$$\tilde{l}^{j,k}_{z,i} = \widetilde{M}^{j,k}_{r,i}\cdot\widetilde{H}^{j,k}_{\theta,i} - \widetilde{M}^{j,k}_{\theta,i}\cdot\widetilde{H}^{j,k}_{r,i}, \tag{44}$$

$$\left\langle\tilde{l}_z\right\rangle^j_{t,i} = \frac{1}{\tilde{t}}\left\{\frac{\Delta\tilde{t}}{2}\left[\tilde{l}^{j,1}_{z,i} + 2\sum_{k=2}^{ndt-1}\tilde{l}^{j,k}_{z,i} + \tilde{l}^{j,ndt}_{z,i}\right]\right\}. \tag{45}$$

3.5. Convergence

Finally, convergence is determined by comparing the current torque value against that of the previous iteration, as shown in Eq. (46). When convergence is achieved, the translational and rotational velocity profiles, $\tilde{v}^n_{\theta,i}$ and $\widetilde{\omega}^n_{z,i}$ respectively, are returned to the user.

$$\left\|\frac{\left\langle\tilde{l}_z\right\rangle_t{}^n - \left\langle\tilde{l}_z\right\rangle_t{}^{n-1}}{\left\langle\tilde{l}_z\right\rangle_t{}^{n-1}}\right\| < \epsilon. \tag{46}$$

4. Illustrative example

Striving to illustrate how the algorithm can be used, we now present an example for the numerical solution of a sample of WBF1 ferrofluid (Table 1), which has been immersed into a container as described by Fig. 1. Such a ferrofluid is subject to an RMF generated by the surface current given in Eq. (47), where K_s stands for the amplitude of current density at the container wall, and m is a uniformity integer that, for a uniform RMF, equals 1.

$$\mathbf{K_s} = K_s\cos\left(\tilde{t} - \theta\right)\mathbf{i_z} = \Re\left\{K_s e^{j(\tilde{t}-m\theta)}\right\}\mathbf{i_z}, \tag{47}$$

Initially, and to validate solutions given by our software (SpinUpFlowDescriptor), we run it for a RMF with low amplitude and frequency. The reason is that, under these conditions, the analytic solutions achieved by other authors are valid [1,2,5]. So, data for v_θ MRSh and ω_z MRSh (Fig. 4) represent the profiles achieved with SpinUpFlowDescriptor. Conversely, v_θ analytic and ω_z analytic stand for the analytic solutions reported in literature [1]. Similarly, v_θ lz0 and ω_z lz0 belong to the numerical solution for the torque at small fields [1]. As Fig. 4 shows, SpinUpFlowDescriptor properly estimates the profiles under these conditions.

After validating our software, we can proceed to simulating moderate values of amplitude and frequency. Under these conditions, analytical solutions lose validity [5]. Fig. 5 shows simulation data for $nder = 30$, $nde\theta = 100$, $ndt = 1000$, a dimensionless

Table 1
Parameters for a ferrofluid sample, including values and dimensions. Modified from [5]. Units are given in the SI.

Ferrofluid WBF1				
Parameter	Symbol	Dimensions	Units	Value
Shear viscosity	η	$\mathrm{M\,L^{-1}T^{-1}}$	mPa s	$1.03 \cdot 10^{-3}$
Viscosity of the carrier liquid	η_0	$\mathrm{M\,L^{-1}T^{-1}}$	mPa s	$1.02 \cdot 10^{-3}$
Magnetic susceptibility	χ	Dimensionless	–	$1.06 \cdot 10^{-1}$
Volumetric fraction	ϕ	Dimensionless	–	$2.13 \cdot 10^{-3}$
Brownian relaxation time	τ_B	T	s	$1.67 \cdot 10^{-5}$
Vacuum permeability	μ_0	$\frac{\mathrm{ML}}{\mathrm{T^2I^2}}$	$\frac{\mathrm{H}}{\mathrm{m}}$	$1.26 \cdot 10^{-6}$
Frequency of the RMF	f	$\mathrm{T^{-1}}$	Hz	$1.50 \cdot 10^{2}$
Cylinder radius	R_0	L	m	$2.47 \cdot 10^{-2}$
Magnetization of the magnetic domain	M_d	$^{\mathrm{I}}/_{\mathrm{L}}$	$^{\mathrm{kA}}/_{\mathrm{m}}$	$4.25 \cdot 10^{5}$
System temperature	T	θ	K	$2.94 \cdot 10^{2}$
Diameter of the magnetic particle	d	L	m	$1.43 \cdot 10^{-8}$
Boltzmann constant	K_B	$\frac{\mathrm{M\,L^2T^{-2}}}{\theta}$	$\frac{\mathrm{J}}{\mathrm{K}}$	$1.38 \cdot 10^{-15}$
κ: no physical meaning	$\kappa = \sqrt{\frac{4\eta\zeta R_0^2}{\eta' \eta_e}}$	Dimensionless	–	3.30
Parameters calculated from the ferrofluid characteristics				
Dimensionless frequency	$\tilde{\Omega} = 2\pi \cdot f \cdot \tau_B$	Dimensionless	–	$1.57 \cdot 10^{-2}$
Vortex viscosity	$\zeta = 1.5 \cdot \phi \cdot \eta_0$	$\mathrm{M\,L^{-1}T^{-1}}$	mPa s	$3.26 \cdot 10^{-6}$
η_e: no physical meaning	$\eta_e = \eta + \zeta$	$\mathrm{M\,L^{-1}T^{-1}}$	mPa s	$1.03 \cdot 10^{-3}$
Zero-order torque	$\left\langle \tilde{l}_{z,0} \right\rangle_t = \frac{\tilde{\Omega}}{1+\tilde{\Omega}^2}$	Dimensionless	–	$1.57 \cdot 10^{-2}$
Sc-sv	$\eta' = \frac{4\eta\zeta R_0^2}{\kappa^2 \eta_e}$	$\mathrm{ML\,T^{-1}}$	kg m $\mathrm{s^{-1}}$	$3.59 \cdot 10^{-8}$

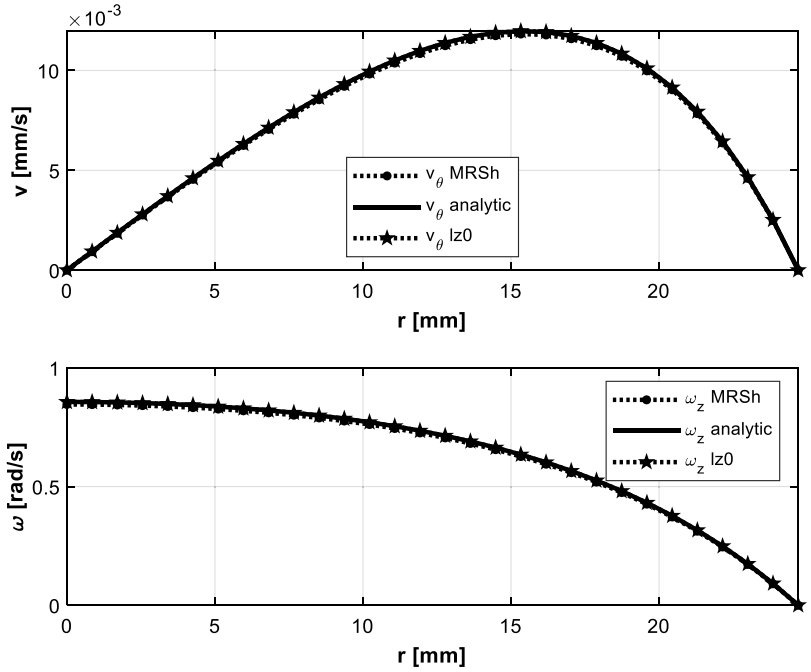

Fig. 4. Validation of the proposed software for the ferrofluid shown in Table 1, while considering a cylindrical container. $\boldsymbol{\alpha = 0.02}$, $\boldsymbol{\kappa = 3.3}$ and $\boldsymbol{f = 150}$ **Hz**. $\mathbf{v_\theta}$ **MRSh** and $\boldsymbol{\omega_z}$ **MRSh** stand for the numerical profiles, while $\mathbf{v_\theta}$ **analytic** and $\boldsymbol{\omega_z}$ **analytic** are the analytic solutions achieved by other authors [1], and $\mathbf{v_\theta}$ **lz0** and $\boldsymbol{\omega_z}$ **lz0** are the numerical solution achieved via the analytic torque value.

simulation time $\tilde{t}_f = 2 \cdot \pi$, and a maximum number of iterations $maxIterT = 100$. This must be given to the software in the following order:

$$\gg \text{SpinUpFlowDescriptor}(nder, nde\theta, ndt, \tilde{t}_f, maxIterT, varargin)$$

where *varargin* relates to two optional inputs, considered as follows:

a. If no argument is given (i.e. length(varargin) = 0), the software carries out a simulation with default parameters. Such a scenario considers magnetic field densities BmT = [3.4 4.5 5.6 6.8 7.9 9.0 10.1 11.3] mT, and the properties of ferrofluid WBF1 (see Table 1),
b. In the case of a single input, it must be a vector of magnetic field densities (in mT) for running the simulation,
c. Should there be two arguments, the first one must relate to the aforementioned vector, whilst the other one must be a

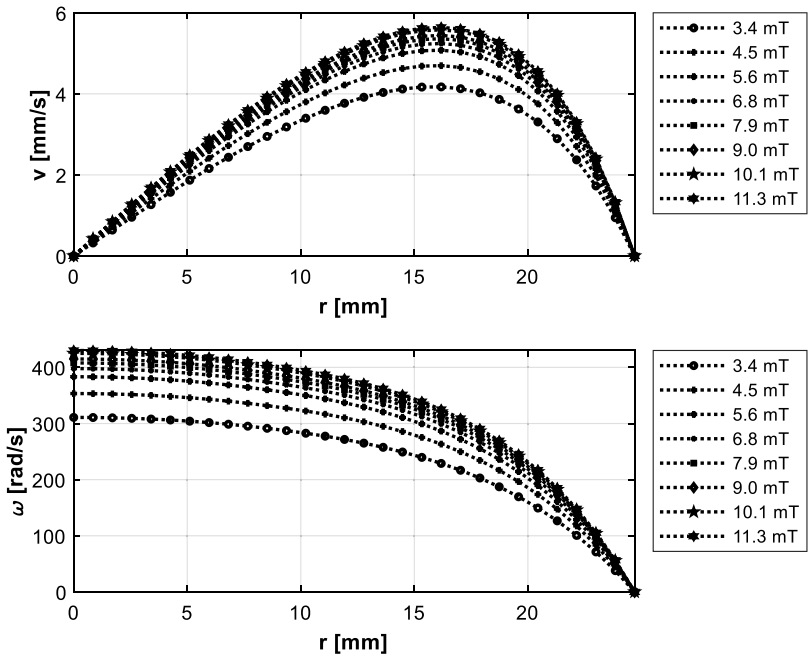

Fig. 5. Translational and rotational velocity profiles for a sample of ferrofluid WBF1, within a cylindrical container, and subject to different densities of an RMF. $f = 150$ Hz, $\kappa = 3.3$.

structure with the parameters of the ferrofluid that will be simulated,

d. Finally, in the case there are three or more arguments, only the first two are considered and must comply with the requirements described in the previous item.

Fig. 5 shows the resulting data for the default scenario, i.e. for $varargin = \{\ \}$, which can be executed with:

$\gg$ SpinUpFlowDescriptor(30, 100, 1000, 2 * pi, 100)

5. Impact and conclusions

By implementing SpinUpFlowDescriptor it is now possible to generate velocity profiles for ferrofluids within a cylindrical container, and under the effect of rotational magnetic fields with medium to high frequencies and amplitudes. Similarly, our software evidences the saturation of velocity profiles. So, increasing magnetic field intensity beyond this point does not incur a rise in magnitude for the profiles. Such a behavior has not been evidenced in the analytical solutions of the simplified model for any kind of geometry. Conversely, the methodology implemented into SpinUpFlowDescriptor considers the relaxation phenomenon of magnetization through equation MRSh-74. This differs from the analytical methodology, which implements equation Sh-72. Since the former describes relaxation phenomena better than Sh-72, it is expected that the profiles given by SpinUpFlowDescriptor agree better with experimental measurements.

Declaration of competing interest

The authors declare that they have no known competing financial interests or personal relationships that could have appeared to influence the work reported in this paper.

Acknowledgment

The authors gratefully thank Universidad Industrial de Santander and Colciencias, Colombia (Grant 567) for the financial support provided to Cristian Jimenez.

References

[1] Chaves A, Zahn M, Rinaldi C. Spin-up flow of ferrofluids: Asymptotic theory and experimental measurements. Phys Fluids 2008;20(5):1–18. http://dx.doi.org/10.1063/1.2907221.

[2] Chaves A, Torres-Diaz I, Rinaldi C. Flow of ferrofluid in an annular gap in a rotating magnetic field. Phys Fluids 2010;22(9):0–15. http://dx.doi.org/10.1063/1.3483598.

[3] Jimenez C, Vargas H, Correa R. Numerical simulation of ferromagnetic fluid flow in a square open channel of infinite axial length under the effect of a rotative magnetic field. Indian J Sci Technol 2018;11(48):1–9.

[4] Jimenez C. Evaluación del efecto de la ecuación de magnetización de martsenyuk, raikher y shliomis sobre las predicciones de flujo de la teoría de difusión de momento angular interno. Universidad Industrial de Santander; 2020.

[5] I. Torres-Diaz, a Cortes, Cedeño Mattei Y, Perales-Perez O, Rinaldi C. Flows and torques in brownian ferrofluids subjected to rotating uniform magnetic fields in a cylindrical and annular geometry. Phys Fluids 2014;26(1):12004. http://dx.doi.org/10.1063/1.4863201.

[6] Jimenez C, Vargas H, Correa R. Velocity profiles of ferrofluids in a cylindrical container and in the presence of external rotating magnetic fields of high strength and frequency. Magnetohydrodynamics 2020;56(4).

[7] Rosensweig RE. Ferrohydrodynamics. Courier Corporation; 2013.

[8] Rinaldi C. Continuum modeling of polarizable systems. Massachusetts Institute of Technology; 2002.

[9] Brenner H. Rheology of two-phase systems. Annu Rev Fluid Mech 1970;2:137–76.

[10] Cowley MD, Rosensweig RE. The interfacial stability of a ferromagnetic fluid. J Fluid Mech 1967;30(4):671–88. http://dx.doi.org/10.1017/S0022112067001697.

[11] Martsenyuk MA, Raikher YL, Shliomis MI. On the kinetics of magnetization of suspension of ferromagnetic particles. J Exp Theor Phys 1974;38(2):413–6.